Supporting information

Reduced lasing thresholds in GeSn microdisk cavities with defect management of the optically active region

A. Elbaz[1,2], R. Arefin[1], E. Sakat[1], B. Wang[1], E. Herth[1], G. Patriarche[1], A. Foti[3], R. Ossikovski[3], S. Sauvage[1], X. Checoury[1], K. Pantzas[1], I. Sagnes[1], J. Chrétien[4], L. Casiez[5], M. Bertrand[5], V. Calvo[4], N. Pauc[4], A. Chelnokov[5], P. Boucaud[6], F. Boeuf[2], V. Reboud[5], J.-M. Hartmann[5], M. El Kurdi[1,*]

[1] Université Paris Saclay, C2N, CNRS, 91120 Palaiseau, France

[2] STMicroelectronics, Rue Jean Monnet 38054 Crolles, France

[3] LPICM, CNRS, Ecole Polytechnique, Université Paris-Saclay, 91128 Palaiseau, France

[4] Univ. Grenoble Alpes, CEA, IRIG-DePhy, 38054 Grenoble, France

[5] Univ. Grenoble Alpes, CEA, LETI, 38054 Grenoble, France

[6] Université Côte d'Azur, CNRS, CRHEA, Rue Bernard Grégory, CS 10269, 06905 Sophia-Antipolis Cedex, France

*corresponding author: moustafa.el-kurdi@u-psud.fr

Table of content:

1. Material growth and characterization

Structural analysis of as-grown layers

The Ge Strain-Relaxed Buffers (SRBs) and the GeSn layers on top were grown in a 200 mm Epi Centura 5200 cluster tool from Applied Materials.[1] Ge SRBs were grown thanks to GeH_4 and a Low Temperature / High Temperature approach, followed by some short duration Thermal Cycling to reduce the threading dislocations densities to values around 10^7 cm^{-2}, typically. Meanwhile, the GeSn layers were grown around 350°C thanks to Ge_2H_6 and $SnCl_4$ precursors. As-grown layers were analyzed by X-ray diffraction Reciprocal Space Mapping. Fig. SI-1 shows the mapping for each sample. The layers are partially relaxed, showing 28.6%, 30.4% and 33.6% of residual compressive strain for samples with 7%, 8.1% and 10.5% of Sn, respectively. 30% of residual strain was therefore adopted for the modeling of the band gap energies of as-grown layer.

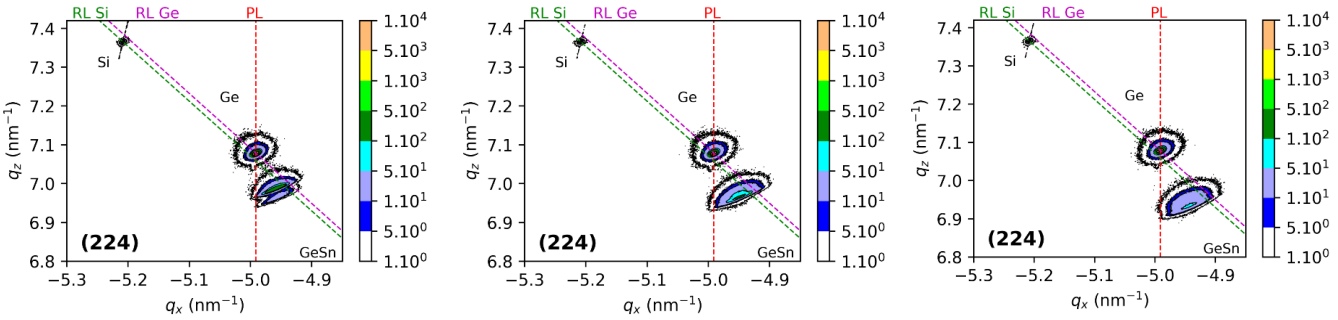

Figure SI-1. Reciprocal space mappings around the (224) X-Ray Diffraction order of the various Sn-content GeSn layers on the Ge SRBs, themselves on Si(001) substrates. Left: 7% Sn. Middle: 8.1% Sn.Right: 10.5% Sn.

Modeling of the band gap energies of as-grown layers

The direct and indirect and gap energies $E_{\Gamma-HH}$ and $E_{\mathrm{L}-HH}$ plotted in figure 2-c were calculated with those equations :

$$E_{\Gamma-HH} = E_{G\Gamma} + (a_c - a_v)\epsilon + b_v\epsilon_{\perp\parallel}$$

$$E_{\mathrm{L}-HH} = E_{G\mathrm{L}} + (a_L - a_v)\epsilon + b_v\epsilon_{\perp\parallel}$$

Where $E_{G\Gamma}$ and $E_{G\mathrm{L}}$ are the direct and indirect band gaps of relaxed alloys as described in the text, a_{c}, a_{L} and a_{v} are the hydrostatic deformation potentials for direct and indirect conduction bands and for valence bands respectively and b_v is the valence band tetragonal deformation potential. We considered a biaxially strained layers with in-plane deformation $\epsilon_{\parallel} = 0.3 \times \frac{a_{Ge} - a_{GeSn}}{a_{GeSn}}$ stemming from the 30% of residual compressive strain. $\epsilon_{\perp\parallel} = \epsilon_{\perp} - \epsilon_{\parallel}$ with $\epsilon_{\perp} = -2\frac{C_{12}}{C_{11}}\epsilon_{\parallel}$ where C_{12} and $C_{11}$are the stiffness constants and $\epsilon = 2\epsilon_{\parallel} + \epsilon_{\perp}$ is the hydrostatic strain.

	Ge	Sn
a_{c}(eV)	-8.24	-6
a_{L}(eV)	-1.54	-2.14
$a_{\mathrm{v}}(eV)$	1.24	1.58
b_v(eV)	-2.9	-2.7
a (Å)	0.565756	0.64912
C_{11} (Pa)	128.53	69.0
C_{12} (Pa)	48.26	29

Table SI-1 Parameter used to calculate the Sn-content dependence of the direct and indirect band gap energies of as-grown layers. [2]

TEM analysis of GeSn microdisks

Transmission electron microscopy (TEM) was used to investigate the crystalline and structural quality of GeSn layers. All GeSn layers analyzed by TEM had thicknesses of 500±10 nm. An additional specific lamella was prepared through a 10µm diameter microdisk, fabricated from the xSn=8% sample, using focused ion beam (FIB) and observed in a FEI Titan TEM microscope operating at 200 keV. Prior to TEM lamella preparation, a dielectric photoresist was spin coated in order to entirely embed the disk in it.

Figure SI-2 shows a Bright Field (BF) Scanning TEM (STEM) micrograph of the microdisk lamella. What appears in bright contrast (white) all around the disk is the spin coated dielectric. Interfaces between the coating dielectric and the GeSn disk surface are abrupt, without any air pocket. Lamella preparation and TEM analysis were performed with standard and routinely used process enabling to qualify the material during its analysis.[3] Currents flux of a few nA were used to image micron-size surfaces, avoiding any additional heating or recrystallization of the defective layers during TEM analysis.[4] We observed, in un-etched area above the Ge pillar, a dense array of misfit dislocations close to the GeSn/Ge interface. In addition, some stacking faults associated with partial dislocations are present on {111} planes. The stacking fault segments merge from the interface at 54° without obviously crossing the entire layer. Some threading dislocations can additionally be observed in this area. In the under-etched area, the dense dislocation network localized near the interface was completely removed. At 165 nm from the Ge pillar, only 34 nm of GeSn were etched but the dense array of misfit dislocations was still removed. From the TEM image in Fig. SI-2 one should obtain roughly 3-4 stacking fault segments per micron along the GeSn/Ge interface that extend over depth more than 60 nm. Some larger stacking faults remain in the suspended layer, but we observed fewer extended defects than above the pillar area

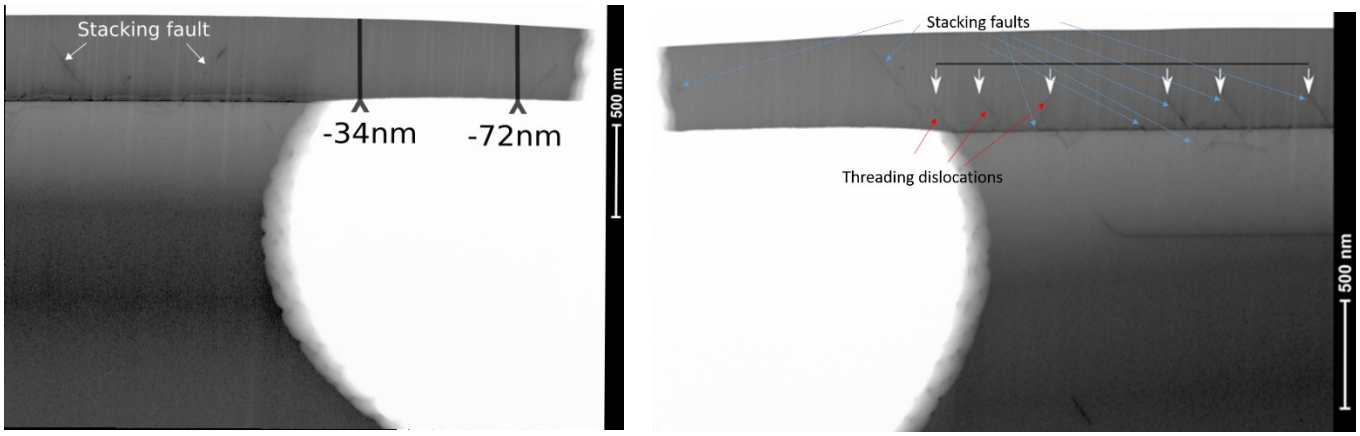

Figure SI-2. BF-TEM image of the GeSn 8% /Ge microdisk. Different types of defects are highlighted.

Raman analysis of strain

The Raman shift measured on 4 µm diameter microdisks for various Sn contents x_{Sn} can be fitted by the general linear law :

$$\Delta\omega = ax_{Sn} + b\varepsilon_{bi}$$

by assuming the layer is fully relaxed ($\varepsilon_{bi} = 0\%$) . We obtained the best fit for the alloy disorder potential $a = -87cm^{-1}$ which is very close to the a parameter measured previously for GeSn alloys, i.e. $-88\ cm^{-1}$in Ref.[5]. The Raman shift of the unprocessed layer, which depends on the alloy disorder and strain (here, 30% of residual compressive strain because of the lattice mismatch with the Ge-VS), is also fitted by including the strain potential parameter b. The value for a is fixed to $-87cm^{-1}$ as obtained from Raman study of microdisks, and only the b value is adjusted to fit measured Raman shifts of as-grown layers. As a result, we obtained $b = -490cm^{-1}$, in very good agreement with the one reported in Ref. [5]. We are thus confident that the residual compressive strain has completely vanished in small diameter microdisks, as also supported by finite element analysis. The inset of Figure SI-3 shows a SEM image of such a microdisk fabricated from a x_{Sn}=10.5% sample. The Raman shift profile along the microdisk diameter shows that strain is very homogeneously distributed.

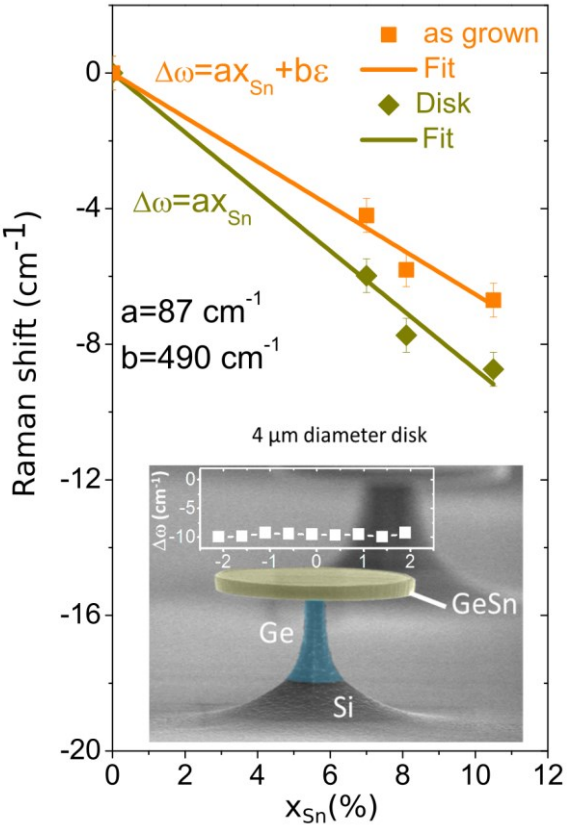

Figure SI-3. Raman shifts for as-grown layers and for suspended microdisks with 4 µm diameters, with respect to the TO phonon frequency of a bulk Ge reference. Continuous lines are linear fits of the data points. The inset shows a SEM view of a fabricated microdisk with a line scan profile of the Raman shift along a diameter.

2. Fabrication

The GeSn layers were processed into suspended microdisks using CMOS-compatible processes, following the following process flow: i) optical lithography was first of all used to define the etching mask for the 7% and 8% Sn-content samples, with an uncertainty of +/-500nm concerning the resulting disk diameter; meanwhile, e-beam was used to define the mask pattern for the sample with 10.5% of tin ii) GeSn layers were etched using Inductively-Coupled Plasma (ICP) etching with a Cl_2, BCl_3, N_2 gas mixture. This anisotropic etching process ensured that the sidewalls of the GeSn microdisks were vertical. After this step the remaining resist mask is not removed, but used to protect the GeSn top surface from the following underetching step

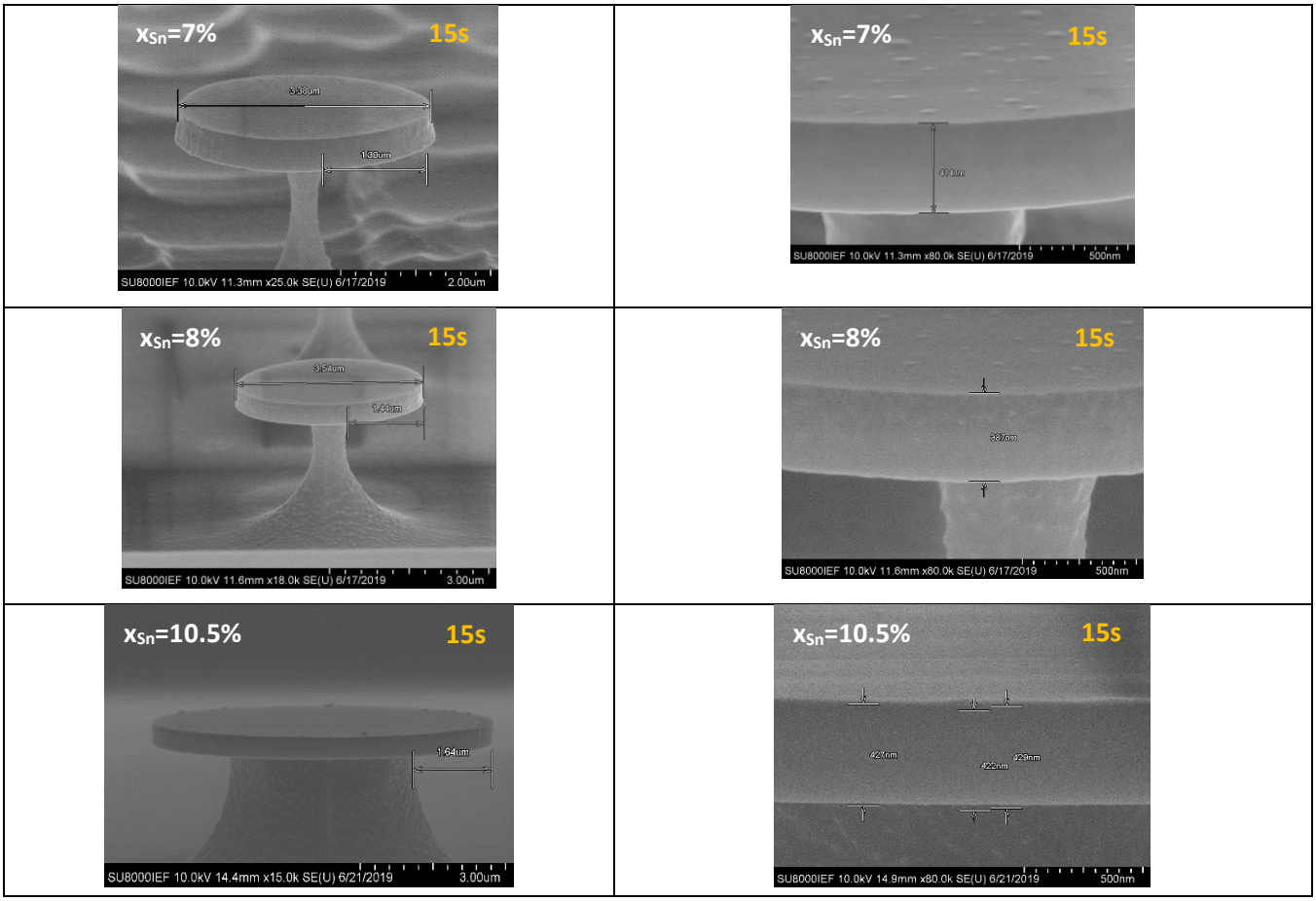

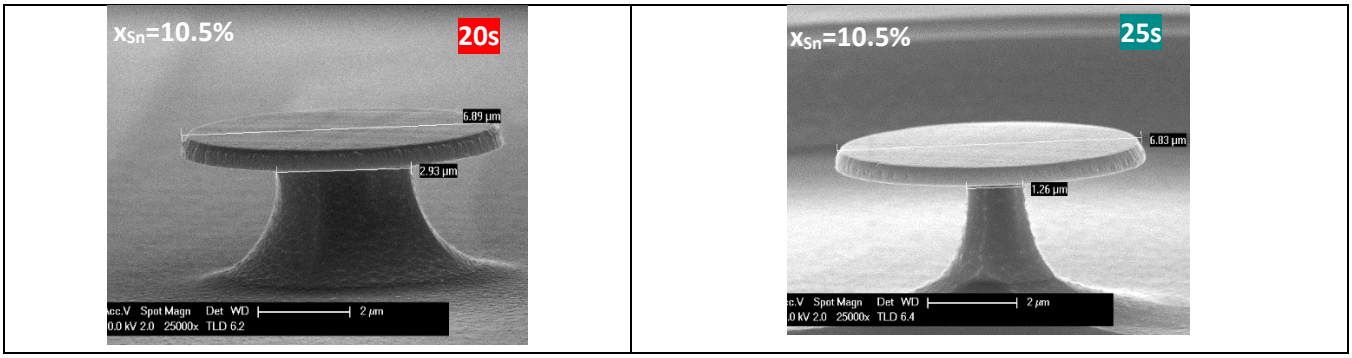

Figure SI-4 SEM images of fabricated microdisks from GeSn layers with 7% (top), 8% (middle) and 10.5% (bottom) of tin (15s of Ge under-etching times). The high magnification images on the right show that the edges of the GeSn microdisks are quite smooth. Those microdisks are thinner close to the edge compared to the as-grown layers they were made from. For the sample with 10.5% of tin, we also show SEM images of microdisks with 7µm diameters and different Ge under-etching times (15s, 20s and 25s), resulting in 1.5 µm, 2 µm and 2.8 µm undercuts, respectively.

A second isotropic plasma etching step using pure sulfur hexafluoride (SF6) gas is used to selectively underetch the Ge layer and form the pillar under the GeSn disk, suspending it above the Si wafer. During Ge etching, the bottom side of the GeSn layer was partially etched. We fabricated samples with Ge under-etching times of 15s, 20s, and 25s, with therefore undercuts (i.e. suspended region sizes) of 1.5 µm, 2 µm and 2.8 µm, respectively. SEM views of fabricated microdisks having undercut of 1.5 µm (for a Ge etching time of 15s) are shown in figure SI-4. The thickness of the GeSn layers at the disk edge is, for all Sn contents, around 400-430 nm, while the thickness of as-grown layers was 490-500 nm.

3. Additional data with different microdisks sizes

We provide additional set of data in Fig.SI-5 for larger disk diameters and under-etching times. We show results (Fig. SI-5a-b-c) obtained at 75 K for a sample with 7% of tin and a microdisk diameter of 7µm but with under-etching times of 15s and 20s, resulting in 1.5 µm and 2 µm undercuts, respectively.
L-L curves show an improvement of the signal and threshold for a larger undercut of 2 µm. This is in good agreement with the observed spectrum dependence with power shown in FigSI-5b and –c for undercuts of 1.5 µm and 2 µm, respectively. On the other hand, the disk with the largest undercut (25s) did not show laser emission. Similar behaviors were obtained with 6 µm diameter microdisks etched from the sample with 8% of Sn (Fig. SI-5d). An increase of the undercut, from 1.5 µm up to 2 µm, resulting in a narrower defective pillar area, may have improved lasing dynamics. Lasing was not achieved for an under-etching time of 25s, however. We indeed observed that an increase of the under-etching time from 15s to 20s resulted in a pronounced thermal roll-over of the L-L curves on Fig. SI-5a and -5d. This is the signature of a reduced cooling of the active region when the pillar is narrower.

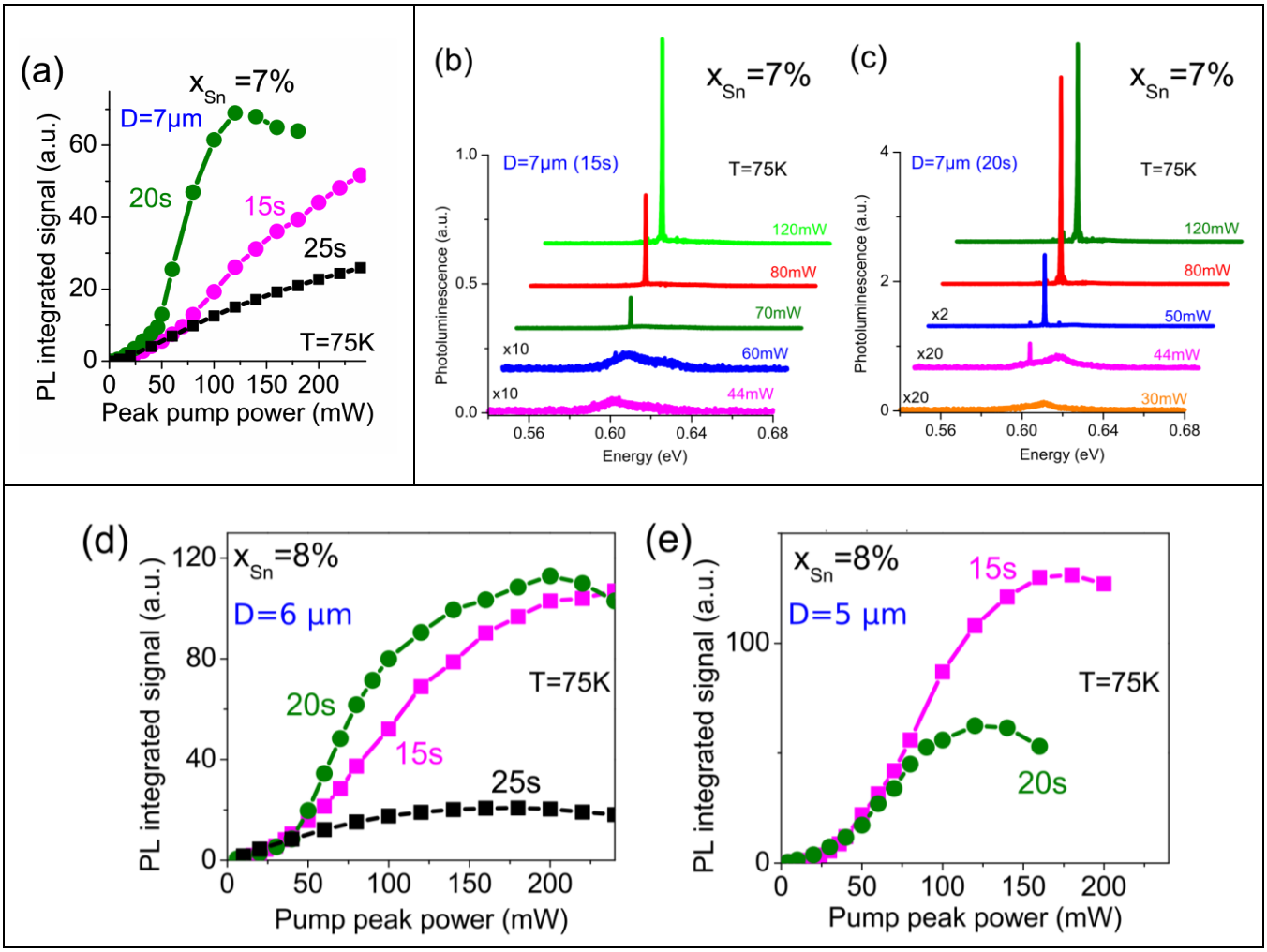

Figure SI-5 (a) L-L curves at 75 K for 7µm diameter GeSn 7% microdisks with 1.5 µm, 2 µm or 2.8 µm under-etches (15s, 20s and 25s of Ge etching times). **(b)** Power dependence PL spectra at 75 K for 7µm diameter microdisks (with 15s of under-etch) **(c)** same as (b) but for a disk with an etching time of 20s **(d)** Same as (a) but for 8% of Sn and a 6 µm disk diameter **(e)** Same as (d) but for a 5µm diameter disk. Microdisks with 25s of etching time were over-etched and collapsed

This behavior is even more marked for the 5 µm diameter microdisk (Fig. SI-5e) which shows that 20s of under-etching results in weaker lasing dynamics than 15s, as the thermal roll-over is more important. These results show the trade-off between the advantages to be had in reducing the pillar area to move defects away from the optically active region and the reduced thermal cooling of the microdisk, which limits lasing.

We analyzed in more details the lasing temperature dependence between 75 K and 90 K for the sample with 7% of Sn. As shown on Figure SI-6, we can clearly observe lasing up to 80-85 K. Very similar maximum lasing temperatures were found for 8 % and 10.5 % of Sn, as discussed in the article.

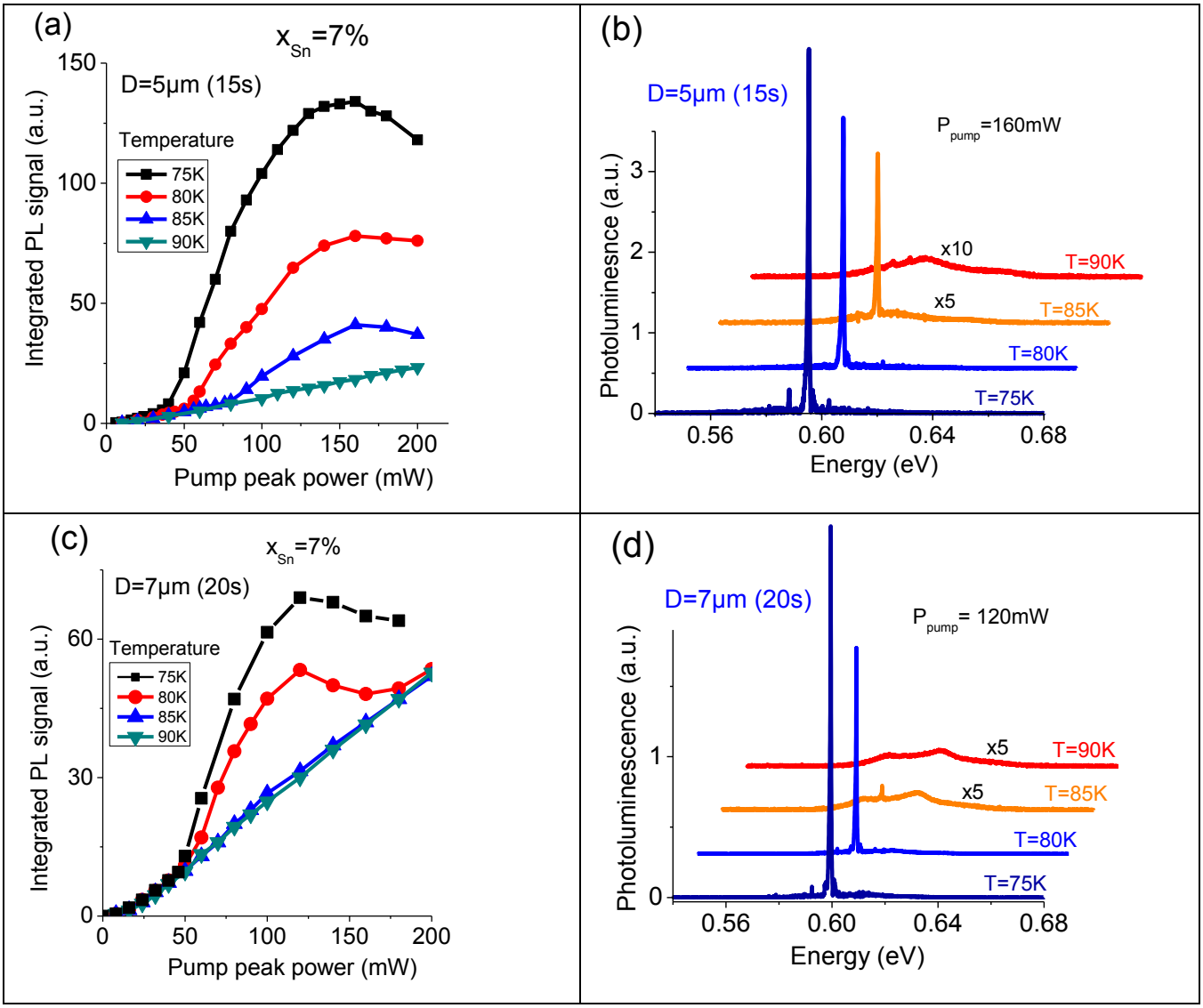

Figure SI-6 (a) L-L curves for x_{Sn}=7% sample measured at temperatures from 75 K to 90 K on 5µm diameter microdisks with 1.5 µm under-etches (15s etching times) **(b)** Temperature dependence of PL spectra at a fixed pump power of 160 mW **(c)** Same as (a) but for a 7 µm diameter disk and a 2 µm under-etch (20s etching time) **(d)** Temperature dependence of PL spectra at a fixed pump power of 120 mW.

We show additional data for the sample with 10.5% of Sn discussed in the text. Fig. SI-7 shows the LL curves and PL spectra for microdisks with 5 µm and 8 µm diameters, both with an under etching time of 15s, yielding an undercut of 1.5 µm. The extracted lasing thresholds at 25 K are 8.9 kW/cm^2 and 11.6 kW/cm^2 for microdisks with 5 µm and 8 µm diameters, respectively. Higher thresholds were obtained for larger microdisks, which might stem from larger defective area above the Ge pillar. Lasing performances are reproducible, the maximal lasing temperature is around 85 K but threshold is reproducibly lower, around 10kW/cm^2, lower than for the disk with a 4 µm diameter discussed in the text.

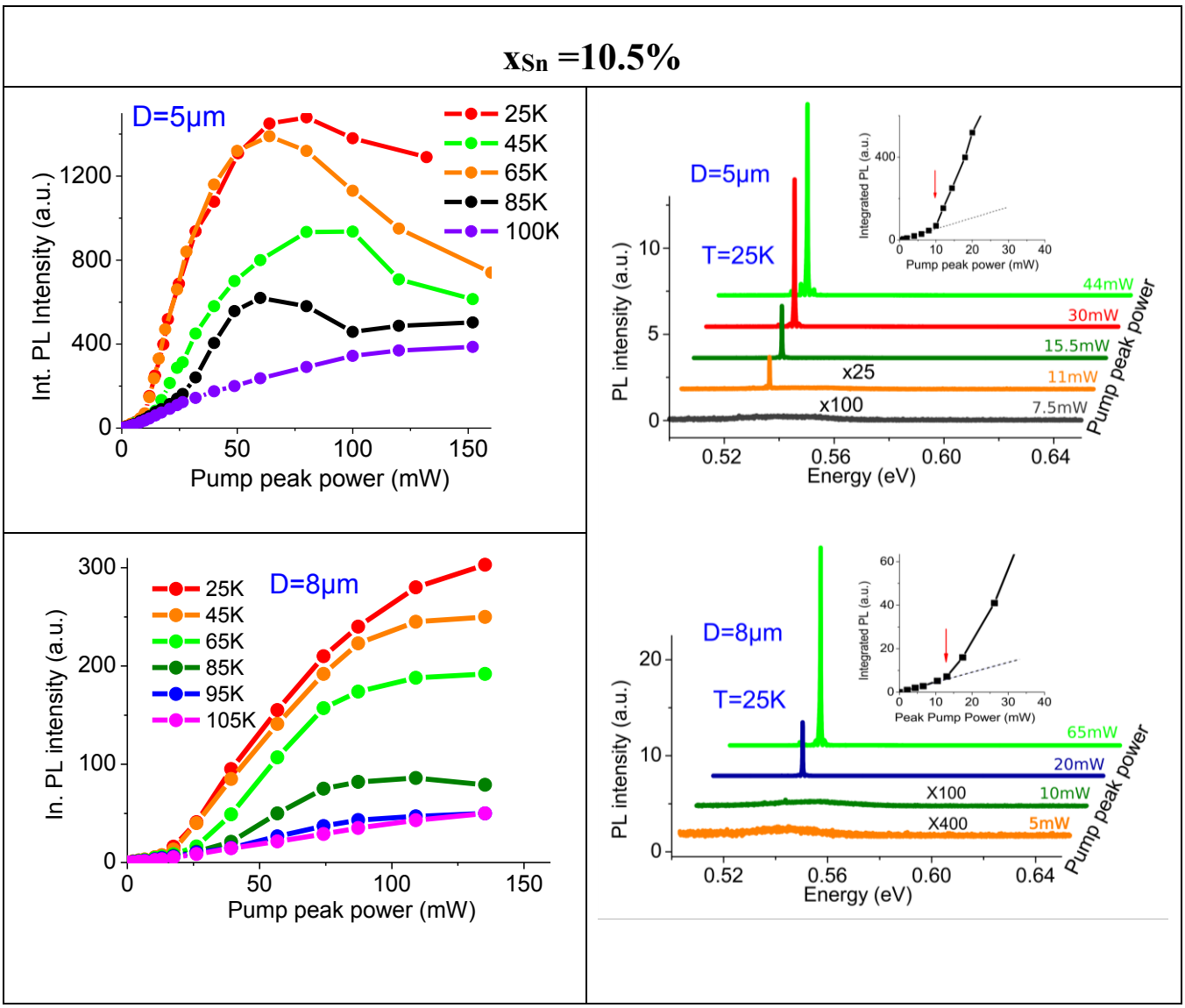

Figure SI-7 L-L curves and low temperature (25K) power dependences of PL spectra for larger diameter microdisks made from GeSn layers with 10.5% of tin grown on Ge SRBs on silicon. The inset in the spectra show a zoom view of the L-L curves near thresholds at low temperature (25K), marked by red arrows.

10 µm diameter microdisks were fabricated from the GeSn 10.5% sample with a process flow similar to that described in the Fabrication section. The SF_6 plasma etching of the Ge pillars was however replaced by a CF_4 plasma etching, as in Ref. [6].The underetching was around 4 µm. To avoid strong heating under optical pumping we thus performed the PL analysis under pulsed pumping with a duty cycle reduced to $3x10^{-5}$. The measured LL curve and PL spectra at 25 K are shown in Fig. SI-8a,b. The lasing threshold is clearly observed for an incident excitation of 145 kW/cm^2, only 4.35 W/cm^2 of average power given the duty cycle. This value is in good agreement with previously reported GeSn microdisks laser thresholds where Ge pillars were etched with CF_4 plasma [3,6].

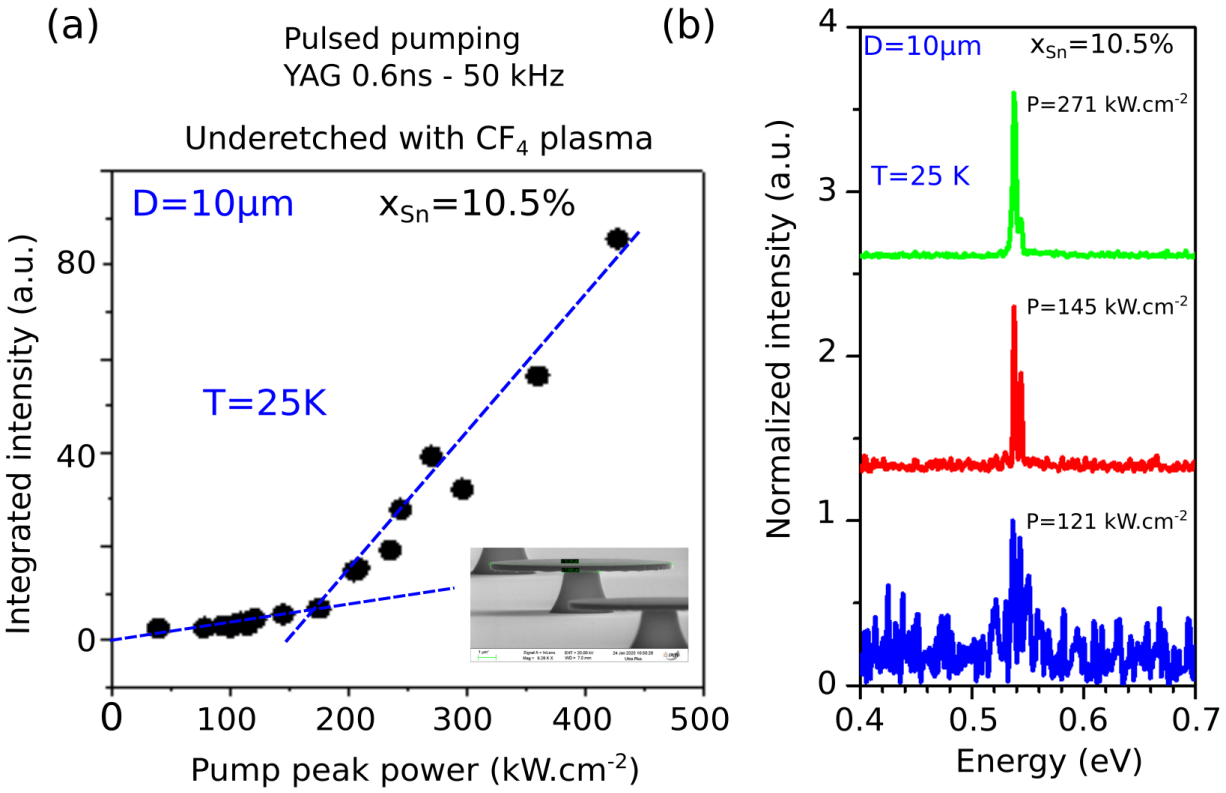

Figure SI-8 (a) LL curve obtained at 25 K from a 10 µm diameter disk with 10.5% of Sn undereched with a CF_4 plasma [6]. The blue dashed lines are drawn to guide the eyes. The insert show a SEM image of such disks **(b)** PL spectra from the disk for different incident pumping powers.

References

[1] J. Aubin, J.M. Hartmann, A. Gassenq, J.L. Rouvière, E. Robin, V. Delaye, D. Cooper, N. Mollard, V. Reboud and V. Calvo, *Growth and structural properties of step-graded, high Sn content GeSn layers on Ge*, Semicond. Sci. Technol. **32**, 094006 (2017)

[2] G.-E. Chang, S. Chang, and S. L. Chuang, *Strain-Balanced $Ge_zSn_{1-z}Si_x/Ge_ySn_{1-x-y}$, Multiple-Quantum-Well Lasers*, IEEE J. Quantum Electron. **46**, 1813–1820 (2010)

[3] D. Stange et. al. , *Optically Pumped GeSn Microdisk Lasers on Si*, ACS Photonics **3**, 1279–1285 (2016)

[4] T. Kimura, M. Ishimaru, M. Okugawa, R. Nakamura and H. Yasuda, *Low-temperature synthesis of crystalline GeSn with high Sn concentration by electron excitation effect*, Jap. Journal of Appl. Phys. **56**, 100307 (2017)

[5] A. Gassenq, L. Milord, J. Aubin, N. Pauc, K. Guilloy, J. Rothman, D. Rouchon, A. Chelnokov, J.-M. Hartmann, V. Reboud, V. Calvo, *Raman spectral shift versus strain and composition in GeSn layers with 6%–15% Sn content*, Appl. Phys. Lett. **110**, 112101 (2017)

[6] V. Reboud, A. Gassenq, N. Pauc, J. Aubin, L. Milord, Q. M. Thai, M. Bertrand, K. Guilloy, D. Rouchon, J. Rothman, T. Zabel, F. Armand Pilon, H. Sigg, A. Chelnokov, J. M. Hartmann, and V. Calvo, *Optically pumped GeSn micro-disks with 16% Sn lasing at 3.1 µm up to 180 K*, Appl. Phys. Lett. **111**, 092101 (2016)